

01 May 2022

Light Emission of Self-Trapped Excitons from Ion Tracks in Silica Glass: Interplay between Auger Recombination, Exciton Formation, Thermal Dissociation, and Hopping

Joseph T. Graham

Missouri University of Science and Technology, grahamjose@mst.edu

Miguel L. Crespillo

Fernando Agulló-López

William J. Weber

Follow this and additional works at: https://scholarsmine.mst.edu/nuclear_facwork

 Part of the [Nuclear Engineering Commons](#)

Recommended Citation

J. T. Graham et al., "Light Emission of Self-Trapped Excitons from Ion Tracks in Silica Glass: Interplay between Auger Recombination, Exciton Formation, Thermal Dissociation, and Hopping," *Acta Materialia*, vol. 229, article no. 117829, Elsevier; Acta Materialia, May 2022.

The definitive version is available at <https://doi.org/10.1016/j.actamat.2022.117829>

This Article - Journal is brought to you for free and open access by Scholars' Mine. It has been accepted for inclusion in Nuclear Engineering and Radiation Science Faculty Research & Creative Works by an authorized administrator of Scholars' Mine. This work is protected by U. S. Copyright Law. Unauthorized use including reproduction for redistribution requires the permission of the copyright holder. For more information, please contact scholarsmine@mst.edu.



Light emission of self-trapped excitons from ion tracks in silica glass: Interplay between Auger recombination, exciton formation, thermal dissociation, and hopping

Joseph T. Graham^{a,*}, Miguel L. Crespillo^{b,c}, Fernando Agulló-López^c, William J. Weber^b

^a Department of Nuclear Engineering and Radiation Science, Missouri University of Science and Technology, 132 Straumanis-James Hall, 401 W. 16th St., Rolla, MO 65409, USA

^b Department of Materials Science and Engineering, University of Tennessee, Knoxville, TN 37996, USA

^c Centro de Microanálisis de Materiales, CMAM-UAM, Cantoblanco, Madrid 28049, Spain

ARTICLE INFO

Article history:

Received 13 January 2022

Revised 4 March 2022

Accepted 5 March 2022

Available online 7 March 2022

Keywords:

Silica

Self-trapped excitons

Ionoluminescence

Ion-matter interactions

Carrier dynamics

ABSTRACT

The initial luminescence yield of amorphous silica under ion irradiation has been studied at temperatures between 30 and 100 K, using swift ions of different masses and energies (3 MeV H, 3.5 MeV He, 19 MeV Si and 19 MeV Cl). The intensity of the 2.1 eV emission band, ascribed to the intrinsic recombination of self-trapped excitons (STEs), has been found to vary systematically with ion mass, energy and irradiation temperature. A detailed model has been developed to quantitatively describe those variations in terms of the competition between non-radiative Auger recombination, STE formation, STE thermal dissociation, and subsequent STE hopping and capture at non-radiative sinks. The model, which uses a thermal spike approach to describe the effect of swift ion bombardment, is found to quantitatively predict the experimental data without adjustable parameters. It provides new insights into the interactions of carriers in an ion track and the behavior of the luminescence emissions during ion irradiation (ionoluminescence). The model is found to predict the correct temperature dependence of the yield if an activation energy for STE thermal migration of 0.12 eV is assumed, which is in good agreement with values previously reported.

© 2022 Acta Materialia Inc. Published by Elsevier Ltd. All rights reserved.

1. Introduction

Luminescence techniques represent an important class of characterization tools for studying the optical and electronic properties of dielectric and semiconductor materials [1]. Compared with other optical characterization techniques such as optical absorbance, Raman spectroscopy, and infrared spectroscopy, luminescence offers superior sensitivity to optically active defects, often by several orders of magnitude. This sensitivity can be attributed to the fact that the visible light detected in a luminescence experiment is the result of outer shell electronic transitions. The energies of such transitions are sensitive to chemical bonding and perturbations in the local chemical environment around defects.

Much information about the upper electronic states of a material, particularly those states within the band gap associated with impurities and defect centers, can be gathered through luminescence measurements. Ionoluminescence (IL) is one such technique that offers unique advantages over the more familiar photolumi-

nescence (PL), cathodoluminescence (CL), and radioluminescence (RL) techniques. As with those other techniques, IL probes the intrinsic or preexisting defects in the material. In addition, the ion species and energy can be chosen to produce defects through radiation damage, allowing the experimenter to study, *in situ* and in real-time, the luminescence emissions from a variable and dynamic population of extrinsic defects. The kinetics of such emissions, when studied over different temperatures, ion stopping powers, and beam currents, provide a wealth of information about color center formation, defect migration, defect clustering, annealing, and the competition between radiative and non-radiative recombination mechanisms [2–10].

Another feature that distinguishes IL from PL, CL, and RL is seen in the electronic excitation density. Swift ions generate carrier densities comparable to or greater than those produced by fs pulsed lasers ($\sim 10^{18}$ – 10^{21} cm⁻³), allowing one to probe the carrier dynamics in an excitation regime inaccessible to PL, CL and RL. Along with fs-laser irradiation experiments, IL is a valuable tool in the study of excitons, Auger recombination, and other multicarrier phenomena seen at high carrier densities. An important difference exists between fs-laser irradiation and ion irradiation. The electronic excitation produced by ions is localized over nm or sub-

* Corresponding author.

E-mail addresses: grahamjose@mst.edu (J.T. Graham), miguel.crespillo@uam.es (M.L. Crespillo), fal@uam.es (F. Agulló-López), wjweber@utk.edu (W.J. Weber).

nm scales perpendicular to the ion path; whereas in laser irradiation, the smallest spatial scale is limited by the diffraction limit ($\sim 1 \mu\text{m}$). Finally, the broad excitation spectrum and high electron-hole densities of IL guarantee the *in situ* and real-time observation of all luminescence bands.

Silicon dioxide (SiO_2) is abundant in nature and finds a multitude of technological uses in both its crystalline and amorphous forms. It is employed in photonics [11–13], microelectronics [14], microelectromechanical systems [15], and nuclear technologies. In several of these areas, such as in laser optics [16], nuclear waste forms [17,18], and nuclear fusion systems [19–22], silica is exposed to high-energy or high-intensity radiation. Consequently, a rich literature on radiation effects in SiO_2 has sprung out of the technological need to understand the material's response to various forms of radiation [5,6,23–40].

Interest in the damage produced by swift heavy ions has grown in recent years due to an accumulation of evidence suggesting that electronic energy loss plays an important role, and in some cases even a dominant role, in damage production in silica. However, the specific damage mechanisms in the electronic energy loss regime are not adequately understood at this time [41]. In silica, as in several other dielectrics, self-trapped excitons (STEs) appear to carry excitation energy from the primary ionizing radiation to the atomic structure or to structural defects in the material [42]. The non-radiative decay of STEs is thought to produce E' centers in silica [43]. STEs may also govern some aspects of latent ion tracks formation in quartz and silica [44]. The luminescence response of silica in the visible spectrum appears to be dominated by STE recombination, either through the direct recombination of the STE, which emits a broad spectrum of photons centered at 2.1 eV, or through its energy transfer and subsequent recombination at non-bridged oxygen hole centers (NBOHCs) and oxygen deficient centers (ODCs), having emissions centered at 1.9 eV and 2.7 eV, respectively.

One of the challenges in properly identifying the intrinsic recombination of the STE and characterizing its emission spectrum is that there is a large degree of overlap of the intrinsic band with the neighboring NBOHC (1.9 eV) and ODC (2.7 eV) bands. These challenges were overcome using cryogenic IL to isolate the 2.1 eV band in low-OH content silica. This allows one to isolate the line shape of the intrinsic STE band and enables quantification of the luminescent yield from STEs in real time. Though much information is contained in the detailed kinetics of the intrinsic and extrinsic emission bands vs. ion fluence, the focus of this work is on the initial yield of light from the 2.1 eV band at low fluence and low temperature. This work will introduce a model that quantitatively predicts the luminescence yield of STEs. The model advances the understanding of key mechanisms governing STE formation in the wake of a swift ion and accounts for the main factors responsible for the decrease in luminescence efficiency with increasing ion stopping power.

2. Methods

2.1. Experiments

Two-side polished IR-grade fused silica glass (SiO_2) samples, with low [OH] content (less than 10 ppm) and 1 mm of thickness, were purchased from Crystran Ltd. and irradiated at the Ion Beam Materials Laboratory at the University of Tennessee, Knoxville [45]. The specimens were mounted on a closed-cycle helium cryostat (Advanced Research Systems, Inc. model DE-204-SF) in a beamline end station under vacuum maintained at or below 6.7×10^{-7} Pa pressure. Beam slits were used to define a square irradiation area between $1 \times 1 \text{ mm}^2$ and $2.5 \times 2.5 \text{ mm}^2$ (depending on ion and energy). The beam was rastered over the slits to maintain beam

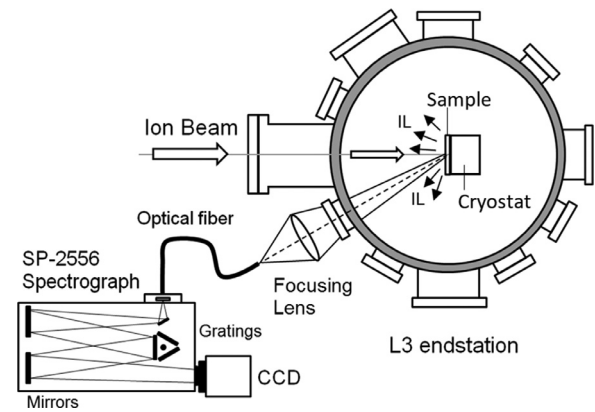


Fig. 1. Experimental setup used to acquire cryo-ionoluminescence (cryo-IL) spectra. Adapted from [10].

homogeneity within 10%. Beam fluxes were between 4×10^{11} and 4×10^{12} particles $\text{cm}^{-2} \text{s}^{-1}$. The source of H, Si, and Cl ions was a solid cathode sputtering target while the helium ions were provided by a radiofrequency plasma source. As such, the 3.5 He beam had the highest flux and lowest current stability. Additional details of the ion sources are provided in [45]. Light was collected at 150° with respect to the beam direction through a sapphire window using a focusing lens and fiberoptic cable. The light was analyzed in a spectrograph (Acton SP-2556) with 0.2 nm spectral resolution and liquid nitrogen cooled charged coupled device (CCD) configured for UV-Vis spectral analysis. Spectra were acquired in 200–1200 ms intervals, depending on the beam current and temperature. Further details of the optical set-up are provided in [10,45,46]. A schematic diagram of the *in situ* experimental set-up is shown in Fig. 1.

Specimen temperatures were monitored by means of a silicon diode sensor mounted onto the sample holder. Commercial vacuum compatible thermal grease with high efficiency at cryogenic temperatures was used to improve thermal contact and temperature uniformity between the bottom of the sample and the sample holder. To reduce charge accumulation on the surface sample during the irradiation, double-sided Cu tape was applied over the edges of the sample surface and sample holder. Nominal irradiation temperatures were 34, 45, 55, 64, 74, 90, and 106 K. However, beam heating effects can be significant, particularly in thermal insulators such as silica at cryogenic temperatures. Thus, the temperature was corrected for beam heating effects using a modified version of the formulas from [47]. Details are provided in Appendix A.

2.2. Data processing

Raw spectra comprised ordered pairs of wavelengths and photon counts binned by wavelength (λ, C_λ). After converting from wavelength to energy binning using an area preserving transformation, a model was fit to the spectra using the Fityk software [48], with the build-in Levenberg-Marquardt algorithm. The model comprised three split Voigt profiles. Spectral samples were used to fit the shape parameters after which the shape parameters were fixed and only the amplitudes were free to vary during extraction of the peak intensities Fig. 2. gives example spectra and peak fits for the lightest ion (3 MeV H) and heaviest ion (19 MeV Cl) at low and high fluence. The figure illustrates that all spectra can be decomposed into three asymmetric components with only three degrees of freedom (peak heights). Similar goodness-of-fit was seen at the higher temperatures. Fourier analysis of the residuals revealed that the maximum low frequency component (attributable to error in the model) was generally less than twice the RMS noise. Uncertainties on the fitting parameters were determined using the

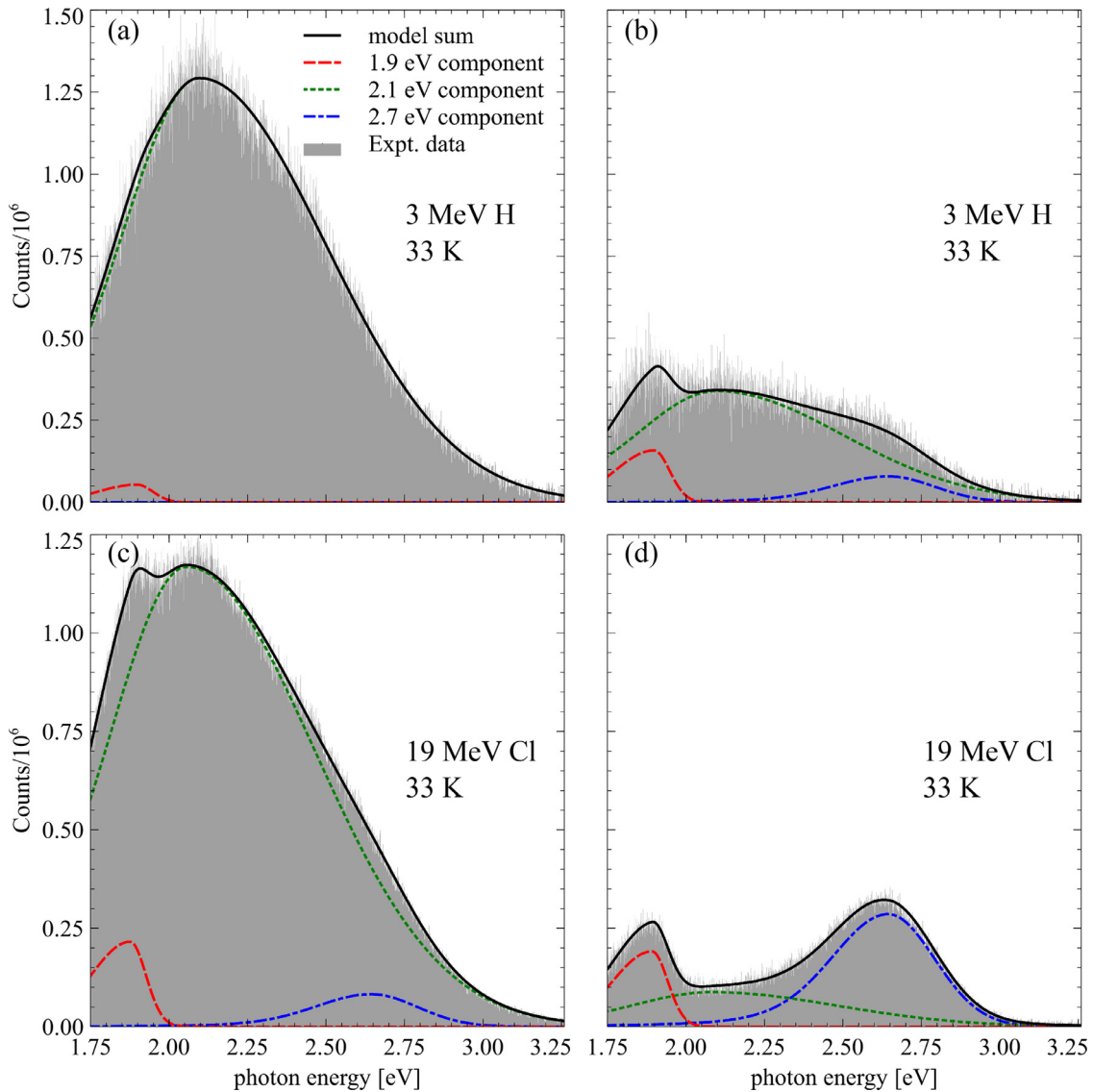


Fig. 2. IL spectra of silica at a nominal temperature of 33 K. (a) 3 MeV H at a fluence of $7.8 \times 10^{11} \text{ cm}^{-2}$ and (b) at a fluence of $6.8 \times 10^{14} \text{ cm}^{-2}$. (c) 19 MeV Cl at a fluence of $5.2 \times 10^{11} \text{ cm}^{-2}$ and (d) at a fluence of $2.0 \times 10^{14} \text{ cm}^{-2}$.

method described in ref. [49]. Uncertainties of derived values were propagated using the quadrature method.

2.3. Modelling

A direct-impact damage accumulation model was assumed [50] and a quenching cross section (σ) and effective track radius (R) were determined from a decaying exponential fit to the yield ($Y_{2.1 \text{ eV}}$) vs. particle fluence (Φ) curve for the 2.1 eV band. In this case, the effective radius defines a cylinder of radius R , within which STEs are effectively removed through non-radiative recombination processes. R is presumably related to the density and non-recombination cross section(s) of enduring structural defects that form along the track.

Because this paper is concerned with the luminescent yield inherent to a single ion track, the analysis was limited to the regime of non-overlapping and isolated tracks. The fitting was only performed using the low fluence data (up to a few $10^{12} \text{ ions/cm}^2$). Beyond $10^{13} \text{ ions/cm}^2$, the amount of overlap begins to become significant, preventing straightforward analysis of the luminescence yield. From this fitting process, it was possible to determine the

initial yield, defined as the intercept of the exponential curve at a zero-fluence.

The model used to study the temperature-, ion mass-, and ion energy-dependent behavior of the luminescence yield in fused silica is based, in part, on the approach of Constantini et al. [28] who adapted the work of Ham [51] on solute atom precipitation to the problem of the luminescence emission of STEs in silica at liquid nitrogen temperature (LNT). The main refinement will be a detailed consideration of the STE source term. The work of Costantini assumed that the initial STE source distribution was proportional to the radial dose distribution. Here that assumption is relaxed and only the interplay between STE formation and Auger recombination is considered. Additionally, the ideas of Bachiller-Perea et al. [31], which suggested that STE yield is also governed, at least in part, by the inelastic thermal spike, have been incorporated into the present model.

2.3.1. STE diffusion equation

The model of Costantini et al. is based on solving the diffusion equation in cylindrical coordinates

$$\partial_t c(r, t) = D \nabla^2 c(r, t) - \frac{1}{\tau_{rad}} c(r, t) \quad (1)$$

where $c(r, t)$ is the radial and time dependent concentration of STEs about the ion track core, τ_{rad} is the radiative lifetime of the STE, and D is the temperature dependent STE diffusivity. The luminescence intensity is then given by the integral of $\frac{1}{\tau_{rad}}c(r, t)$ over radii and time.

Non-radiative losses at radiation-induced structural defects are incorporated through an absorbing boundary condition at the effective radius, R . For $r \leq R$, the STE concentration is zero, and the light yield is zero, due to the high quenching probability in that region. A larger radius, R_0 , is defined through the following expression based on Ham's and Costantini's treatment:

$$\frac{\pi R^2}{\pi R_0^2} = 1 - \exp(-\pi R^2 \Phi) \quad (2)$$

where R_0 is a measure of track separation. In the limit of low fluence, πR_0^2 is the area per track (inverse of the fluence). R_0 appears in the calculation of the yield as the upper bound on the integral of $\frac{1}{\tau_{rad}}c(r, t)$. In other words, STEs that diffuse away from a track core and beyond a distance, R_0 , will have wandered into the neighborhood of a nearby track where they have a chance of being absorbed by the inner quenching region. In these experiments, Φ was taken to be the accumulated fluence during the first spectral acquisition, i.e. the particle flux times the acquisition time. The R_0 and R parameters were not found to have a large qualitative effect for the lowest temperature data (33 and 45 K). Given that the yields are extrapolated to zero fluence, it might seem more logically coherent to take $R_0 \rightarrow \infty$ (macroscopically separated tracks). At higher temperatures, however, the STE diffusion lengths are comparable to the mean track separation at the end of the first spectral acquisition and therefore, assuming perfectly isolated tracks is not consistent with the experimental reality.

Luff and Townsend [52] showed that τ_{rad} for quartz is nearly constant and equal to about 1 ms below 150 K but decreases above 150 K due to competition from non-radiative mechanisms. Itoh et al. [24] measured a decay time of 0.94 ms at 195 K for the 2.5 eV STE band in quartz (corresponding to the 2.1 eV STE band in silica). As the experiments analyzed here were conducted at temperatures below 150 K, a value of 1 ms was assumed. Following Costantini et al. [28] and Bachiller-Perea et al. [31], it is assumed that STEs migrate through a hopping process that obeys standard Arrhenius behavior. The migration energy has been estimated to be around 0.1–0.12 eV [28,53]. The STE can be approximately thought of as a bound state of an electron and self-trapped hole, with the electron localized on the Si atom and a hole localized on neighboring oxygen in the SiO_4 tetrahedron [54]. The STE's mobility is essentially governed by that of the self-trapped hole [55].

The preexponential factor in the STE diffusivity was estimated to be $0.010 \text{ cm}^2 \text{ s}^{-1}$ based on the maximum vibrational frequency, around 1200 cm^{-1} for SiO_2 [56–59], a geometry factor of $2/\sqrt{3}$ for tetrahedral hopping, and a hopping distance equal to the mean Si-Si nearest neighbor distance ($\sim 3 \text{ \AA}$) [60]. For a migration energy of 0.1 eV, the diffusion length over a STE lifetime is $\sim 0.2 \text{ \AA}$ at 33 K. Thus, one may regard STEs to be immobile at the lowest temperatures studied in the experiment. This fact will become useful later in separating the initial STE survival fraction from STE diffusion effects in the yield data.

Given an initial STE radial distribution, Eq. (1) can be numerically solved and the luminescence yield determined. While it may be reasonable to consider the initial concentration of electron-hole pairs to be proportional to the ionization dose, formation of STEs depends in a rather complex way on the interplay of several mechanisms that are carrier density and temperature dependent. These mechanisms are now considered.

2.3.2. Radial concentration of STEs

To model the initial radial concentration of STEs one must consider their formation, dissociation, and the non-radiative recombination mechanisms that might compete with STE formation. The latter effects have been considered in a phenomenological way by Muga and Griffith [61] and by Michealian and Menchaca-Rocha [62] through the incorporation of a characteristic radius (either termed a saturation radius or quenching radius). Here a different approach is taken and basic physical parameters for silica, gathered from the literature, were used to construct a model that attempts to describe the underlying physics.

The initial distribution of free carriers is assumed to be

$$n_c(r, 0) = \frac{1}{2.5E_g}X(r) \quad (3)$$

where the factor $2.5E_g$ is used to estimate the mean excitation energy for the dielectric [63]. $X(r)$ is the radial dose distribution created by delta electrons. $X(r)$ was calculated using the formula of Katz et al. [64] with Waligorski et al.'s empirical correction factor [65] and using Fageeha et al.'s density correction [66].

Upon their creation, the charged carriers may begin to recombine, diffuse, become self-trapped, or form excitons. On the other hand, carrier densities can be high, especially at the center of the track, and so non-radiative Auger recombination must be considered. For time scales after the initial electron-hole plasma has formed, the concentrations of charged carriers, n_c , and STEs, n_{STE} , obeys the following coupled equations:

$$\begin{aligned} \partial_t n_c &= D_a \nabla^2 n_c - \frac{1}{\tau_{STE}} n_c - C n_c^3 + \frac{\Gamma}{\tau_{STE}} \frac{n_{STE}}{n_c} \\ \partial_t n_{STE} &= \frac{1}{\tau_{STE}} n_c - \frac{\Gamma}{\tau_{STE}} \frac{n_{STE}}{n_c} \end{aligned} \quad (4)$$

D_a is the ambipolar diffusion coefficient for free carriers, τ_{STE} is the STE formation time, C is the coefficient for Auger recombination. The final term represents thermal dissociation of STEs. Γ is an equilibrium constant that depends on the temperature of the electron-hole plasma during the inelastic thermal spike. A derivation of the dissociation term is provided in Appendix B. The dissociation constant is implicitly a function of radius and time as it depends on the evolution of the electronic temperature near the track core. The inelastic thermal spike evolves over short time scales (fs to ns) and spatial scales (Angstroms to tens of nm). As such, there are regions in the ion track where the relative rates of Auger recombination, STE formation, and STE dissociation evolve dynamically over the lifetime of the thermal spike.

Estimates of the ambipolar carrier diffusivity D_a can be made by considering the mobilities of electrons and holes. Conduction electrons are quite mobile in SiO_2 [67–69]. Due to hole self-trapping however, the hole mobility is several orders of magnitude lower [70,71]. Moreover, since the STE can be approximately envisaged as a carrier that forms when a free electron binds to a self-trapped hole, it is only the self-trapped hole mobility that one need to consider [55]. The effect is that the ambipolar diffusivity term in Eq. (4) is approximately equal to the diffusivity of the self-trapped holes. The corresponding diffusion lengths over the timescales of STE formation and Auger recombination are considerably smaller than the track size for temperatures less than 1000 K. Therefore, in the case where the track core stays relatively cold, the diffusivity term in Eq. (4) can be ignored.

The STE formation time has been measured using pump-probe laser techniques and has been found to fall in the range of 50–200 fs, with most studies reporting a lifetime around 150–170 fs [72–75,77–79,76]. The lifetime appears to be only weakly dependent on the carrier concentration. One can note that the shortest measured time 50 fs [78] had a larger initial carrier concentration ($> 8 \times 10^{20}$

cm^{-3}) than most of the other studies, which reported densities on the order of $1 \times 10^{20} \text{ cm}^{-3}$ or lower. A similarly short lifetime, 60 fs, reported by Li et al. was measured at excitation densities near the Optical Breakdown Threshold [75]. Thus, there is some limited evidence of a weak carrier density dependence in τ_{STE} . Indeed, one typically expects that exciton formation follows bimolecular kinetics. That said, it is unlikely that the relaxation time can continue to decrease further with increasing carrier concentrations as STE formation (or self-trapped hole formation) requires atomic relaxation, which cannot be much faster than the reciprocal of the Debye frequency. Thus, it may be the case that at these high excitation densities, the rate of STE formation limited by atomic relaxation. For the purposes of the calculation, it is assumed that $\tau_{STE} = 150 \text{ fs}$.

2.3.3. Auger recombination

For traditional semiconductors, the Auger coefficient, C , is known to have a strong temperature and bandgap dependence for direct bandgap materials with bandgaps smaller than about 1 eV. For indirect bandgap semiconductors and direct bandgap semiconductors with bandgaps greater than 1 eV, C takes on a nearly constant value around $10^{-30} \text{ cm}^6 \text{ s}^{-1}$, give or take an order of magnitude [80]. The trend in traditional semiconductors is represented in Fig. 3(a). For indirect bandgap materials, there is little temperature dependence [81,82]. If one looks beyond III-V and IV semiconductors, the situation appears to be quite different. The role of the relative permittivity is rather prominent. Though the literature on Auger recombination in insulators and glasses is quite sparse, one can see a clear trend in the Auger coefficient with relative permittivity (Fig. 3(b)). Auger recombination is mediated by the screened Coulomb interaction. As such, carriers that experience relatively little screening (low permittivity) tend to exhibit larger Auger coefficients than materials with high permittivity. Disorder and confinement effects have also been shown to dramatically enhance Auger recombination [82,83]. Silica has a moderately low relative permittivity (3.7–3.9) and no long-range order. Thus, one might expect silica to have a considerably higher Auger coefficient than $10^{-30} \text{ cm}^6 \text{ s}^{-1}$. Indeed, from Fig. 3(b) it appears that the coefficient most likely lies in the range of $10^{-28} - 10^{-26} \text{ cm}^6 \text{ s}^{-1}$. $C = 10^{-27} \text{ cm}^6 \text{ s}^{-1}$ is used in the present calculations.

2.3.4. Thermal spike calculations

Because the STE dissociation constant depends on the electron temperature during the inelastic thermal spike, separate thermal spike calculations were performed for each combination of ion, energy, and stopping power using the code of Dufour et al. [91]. The code numerically solves the heat equation for the electron temperature and lattice temperature following excitation of the electronic system by a radially varying source term (the ion). The source term is based on the Waligorski model. Equilibrium thermal properties are assumed for the lattice. Excited electrons, on the other hand, are treated as hot electrons in a metal as their concentrations are large and governed by ion impact rather than by Fermi-Dirac statistics at thermal equilibrium. The two heat equations are coupled through an electron-phonon coupling term. The coupling term is assumed to be constant. An electron-phonon mean free path of 3 nm was used, as it was found to provide a good fit to measured ion track radii in silica [92]. However, it was shown that for materials with a band gap, the electron-phonon coupling is highly dependent on the local electron temperature and thus may significantly affect the radial temperature profile, particularly over short time scales [93]. Therefore, with its many assumptions, the effects of the thermal spike term on the results may be more qualitative than quantitative.

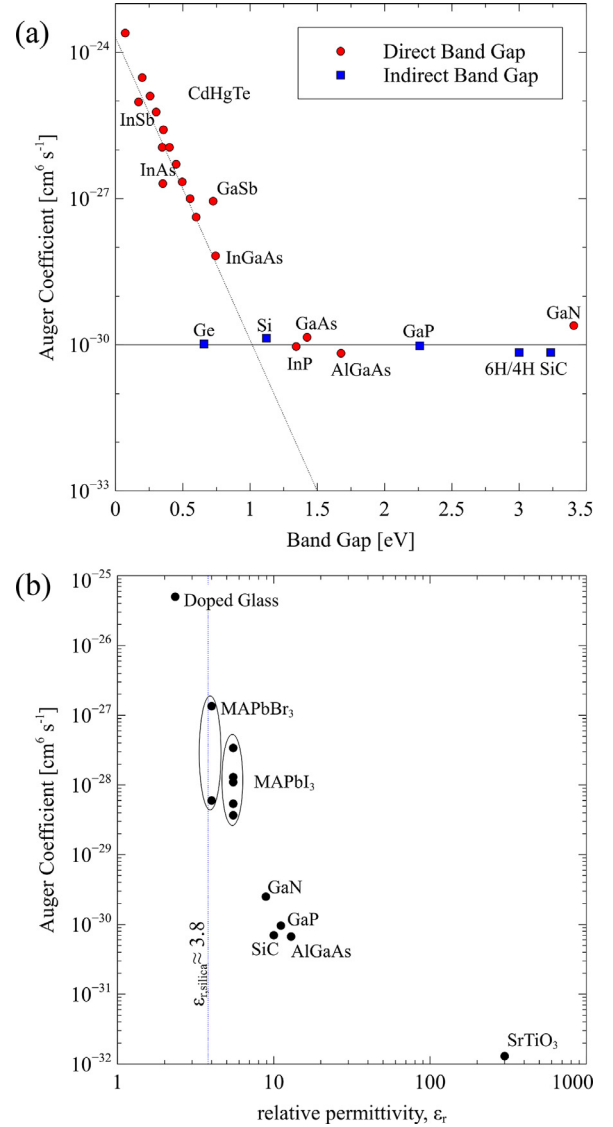


Fig. 3. (a) Auger recombination coefficient of traditional direct and indirect semiconductors. Adapted from [80]. (b) Auger recombination coefficient of semiconductors with energy gap > 1 eV and several insulators [84–90]. The blue line indicates the relative permittivity of silica glass. (For interpretation of the references to color in this figure legend, the reader is referred to the web version of this article.)

2.3.5. Calculation of the luminescence yield at low temperature

Eq. (4) was numerically integrated for different ion energies and electronic stopping powers spanning the ion range (i.e. 0 MeV to the incident ion energy). Stopping powers were calculated using the Stopping and Range of Ions and Matter (SRIM) code, ver. 2013 [94]. The Waligorski/Katz radial dose distributions were normalized to the SRIM values, as SRIM stopping powers are likely more accurate. The Waligorski/Katz model is essentially a classical model and does not include important effects such as the shell-correction.

As mentioned above, at 33 K, STEs are immobile. Thus, the initial yield data at 33 K only depends on the radial distribution of STEs. The STE yield was calculated using

$$Y = \int_0^{E_{init}} \frac{dE_{ion}}{S_e(E_{ion})} \int_R^{R_0} n_{STE}(r, t; E_{ion}, S_e, M_{ion}) 2\pi r dr \quad (5)$$

where $n_{STE}(r, t; E_{ion}, S_e, M_{ion})$ is the radial concentration of STEs. Note that the STE concentration depends on the ion mass (M_{ion}), energy (E_{ion}) and stopping power (S_e). The radial distribution of

Table 1

Ion track radii, maximum electronic stopping power ($S_{e,max}$), and maximum nuclear ($S_{n,max}$) stopping power.

Energy/ion	Effective Radius [nm]	$S_{e,max}$ [keV nm ⁻¹]	$S_{n,max}$ [keV nm ⁻¹]
3 MeV H	1.2	0.12	0.001
3.5 MeV He	2.1	0.34	0.011
19 MeV Si	2.4	3.48	0.445
19 MeV Cl	4.4	4.14	0.565

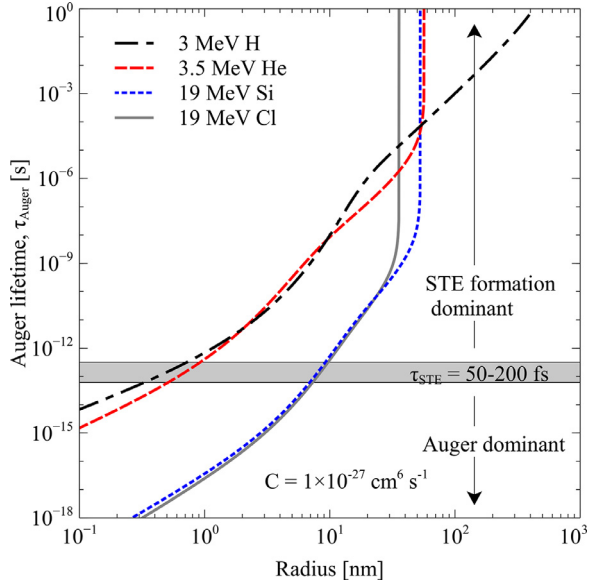


Fig. 4. The radial variation in Auger lifetime for 3 MeV H, 3.5 MeV He, 19 MeV Si, and 19 MeV Cl.

electron-hole pairs and the temperature evolution of the inelastic thermal spike varies along the ion trajectory. This gives rise to variations in the relative amounts of Auger recombination, STE formation, and thermal dissociation. For higher temperatures, the effects of STE migration must also be included in an additional step.

$$Y = \int_0^{E_{init}} \frac{dE_{ion}}{S_e(E_{ion})} \int_{10 \text{ ps}}^{\infty} \int_R^{R_0} \frac{1}{\tau_{STE}} n_{STE}(r, t; E_{ion}, S_e, M_{ion}, T) 2\pi r dr dt \quad (6)$$

n_{STE} is evolved both through Eq. (4) and the diffusion equation (Eq. (1)) up to timescales of $10\tau_{STE}$. A strong absorbing boundary condition is imposed at $R(n_{STE}(R, t) = 0)$. Note that the lattice temperature, T , now appears as it does in the STE diffusion equation (Eq. (1)).

3. Results and discussion

The effective radii determining by fitting the low fluence kinetics curves (at 33 K) are given in Table 1, along with the maximum electronic stopping powers ($S_{e,max}$) and maximum nuclear stopping powers ($S_{n,max}$). As one might expect, the size of the quenching region is correlated with stopping power (electronic, nuclear, or total). The larger energy density, the greater the number of radiation-induced defects that quench STEs through non-radiative recombination processes.

A plot of the radial dependence of the initial Auger recombination lifetime, $\tau_{Auger} = 1/Cn_c^2$, is shown in Fig. 4. Overlaid is the STE formation lifetime. This figure shows that for each ion there is an inner radius region where the excitation density is so high that the kinetics will initially be dominated by Auger recombination surrounded by a lower density region dominated by STE formation. The cutoff radius appears to have a strong dependence on

ion energy and mass, explaining a large contribution to the drop off in luminescence efficiency with stopping power.

The calculated STE distributions at the end of the STE formation phase (10 ps) and prior to the STE diffusion phase are shown in Fig. 5 as solid lines. The initial carrier concentration is shown as dotted lines. One sees that the STE concentration reaches its maximum at approximately the radius where the Auger recombination rates and STE formation rates are equal to each other. At this point, the maximum STE density is around 10^{20} cm^{-3} . Interestingly, near the center of the track there is a depression in the STE concentration, most notably for 19 MeV Si and Cl, though also present for 3.5 MeV He. The cause of this depression is more apparent when one examines the thermal spike calculations, two examples of which are shown in Fig. 6. Fig. 6a shows the electronic temperatures at the center, 1 nm away from the center, and 5 nm away from the center of a 3 MeV proton trajectory. The small spatial extent of the thermal spike and its relatively low temperatures prove to be insufficient to ionize a significant fraction of STEs at any point in the STE formation process. In contrast, the highest stopping power ion, 19 MeV Cl, shown in Fig. 6b, is capable of raising the temperature to thousands of degrees within the first few nm of the track. Most importantly, the peak temperatures are reached at timescales comparable to the STE formation lifetime. At this point, one expects there to be competition between Auger recombination and STE formation. The effect of dissociation at that timescale is to continuously ionize the newly formed STEs, giving the charged carriers additional opportunities to disappear through non-radiative Auger recombination. Hence, the higher core temperatures achieved with heavy ions are responsible for the central dip in the STE distribution. The thermal spike was found to only contribute to 0.37% of Auger recombination for 3 MeV H and 5% for 3.5 MeV He. For 19 MeV Si, and 19 MeV Cl the contributions were 39% and 28%, respectively. Thus, for heavy ions, STE/e-h equilibrium shifts during the thermal spike appear to have a significant effect on the radiative emission yield; while for light ions, there is not enough heating to dissociate an appreciable number of STEs.

These results are compared to the experimental values in Fig. 7. In both cases, the yields were normalized to the yields for protons, since only relative yields (not absolute) can be measured in the experimental setup. Despite the many simplifying assumptions contained in the model, it produces results that are in surprisingly good quantitative agreement with the experimental data. It should be reiterated that, up to this point, the model contains no adjustable parameters. All parameters are based on experimental measurements in silica or are estimated from experimental parameters measured in similar materials and reported in the literature. The STE dissociation rate has its own additional theoretical considerations. Its derivation assumes that STEs are essentially low energy conduction band electrons bound to self-trapped holes with a well-defined binding energy. For the purposes of the model, a typical value of the STE thermal quenching energy for quartz was used, 0.2 eV [95]. In glasses, the binding energy is described by a distribution, rather than a single value [95]. However, in performing the simulations, it was noted that varying the value of the STE binding energy from 0.1 to 0.3 eV did not alter the yields by more than a few percent, and increasing the binding energy up to 0.6 eV (corresponding to one estimate of the STE binding energy in silica [60]) only increased the yield by 22% for the hottest track (19 MeV Cl). For the light ions, STE dissociation only plays a small role in the yield, and hence little effect can be seen by varying the binding energy. Thus, within a realistic range of binding energy values, the yield is not strongly dependent on STE binding energy for the ion energies and masses studied. It is possible that for higher stopping power ions, with low velocities (i.e. energetic high-Z ions or clusters), a greater effect could be observed.

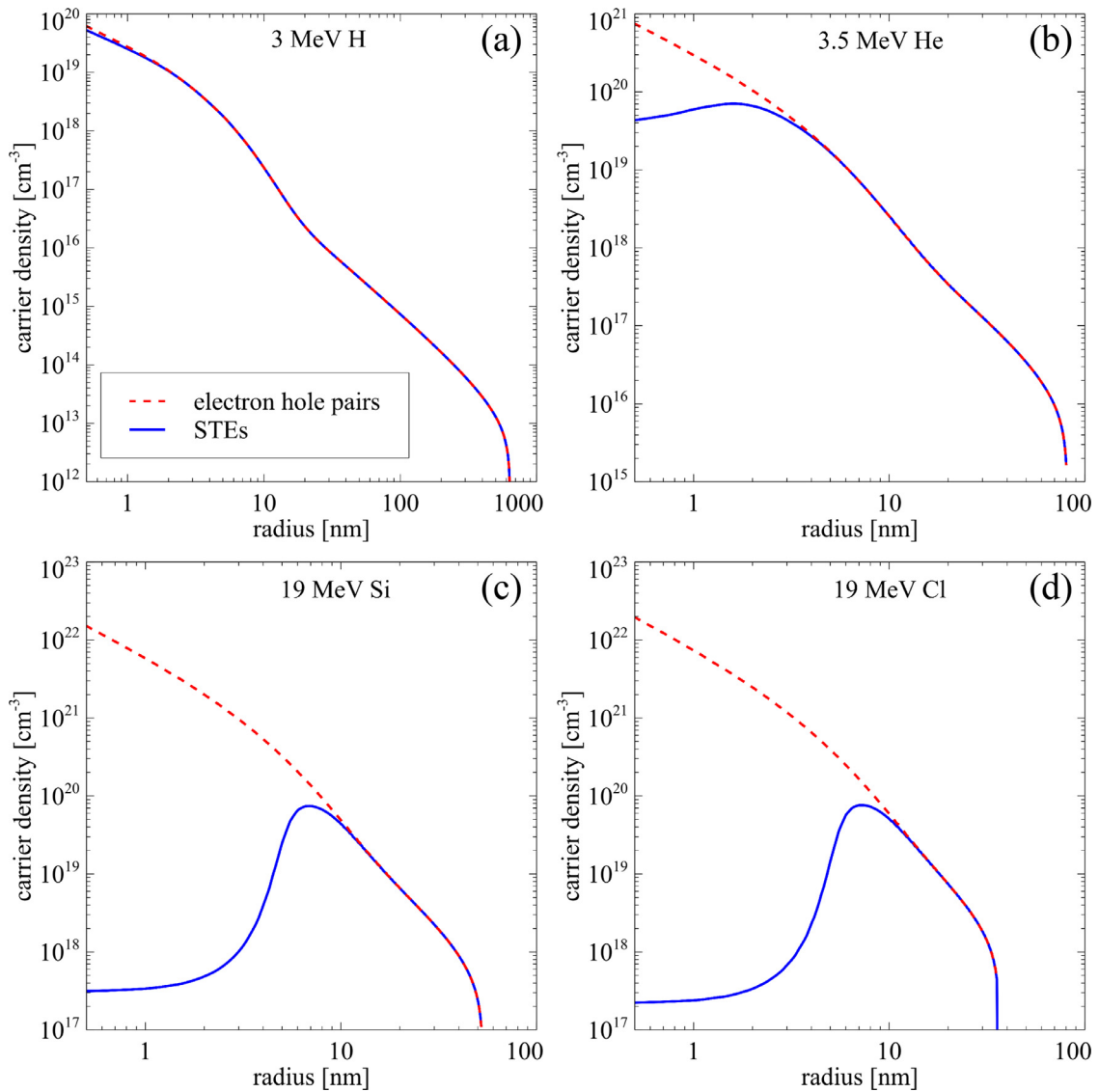


Fig. 5. Radial distribution of surviving STEs (solid blue line). The initial density of e-h pairs is shown by the dashed red line. (For interpretation of the references to color in this figure legend, the reader is referred to the web version of this article.)

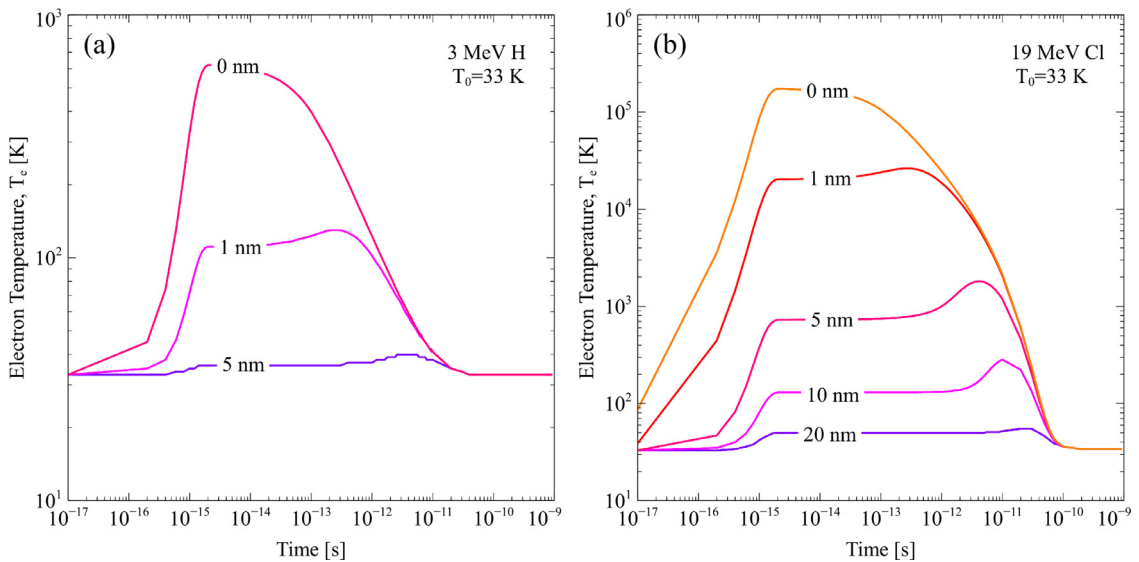


Fig. 6. Inelastic thermal spike calculations of electronic temperature T_e as a function of time for 3 MeV H and 19 MeV Cl. Each line indicates the temperature evolution at a fixed radius from the center of the track.

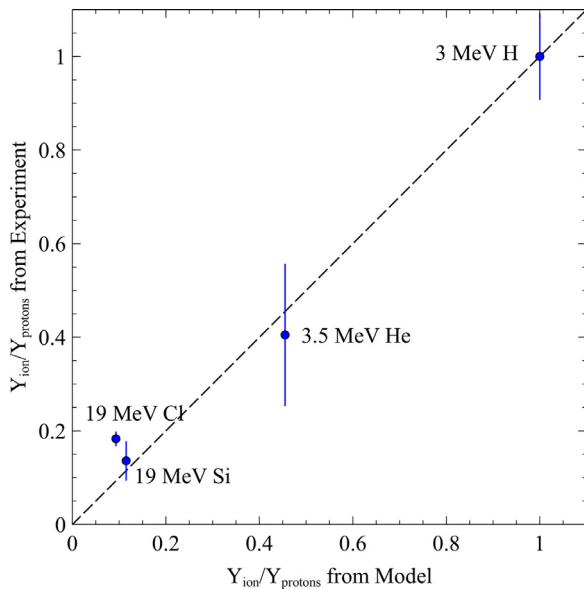


Fig. 7. Measured and predicted ion luminescence yield relative to 3 MeV protons from the 2.1 eV emission band. Error bars represent the standard error.

Finally, shown in Fig. 8 is the initial yield vs. temperature from the 2.1 eV emission band for 19 MeV Si and 19 MeV Cl. The blue data points show the normalized yield vs. the temperature measured on the cryostat. The model with a 0.08 eV STE migration energy (solid blue line) agrees reasonably well with these data. However, due to beam heating effects, the actual temperatures in the luminescent area are significantly higher. The red points contain the same intensity data values as the blue markers, but the temperatures are shifted through the beam heating correction. The beam heating correction gives something of a theoretical maximum temperature. The true temperatures lie between the two datasets but close to the corrected (red) values. With the temperature correction, reasonable agreement is found for a migration energy of 0.12 eV (dashed red curve). With this data alone, it is not possible to provide a precise estimate of the STE migration energy, but it is around 0.12 eV. These results corroborate those of

Costantini et al. [28] who estimated a STE migration energy around 0.1 eV and Zhang and Ong [53] who estimated an STH migration energy around 0.12 eV. One can see that the model predicts a complete quenching of the light at 100 K. This is due to the strong absorber boundary condition, which amounts to assuming that the STE undergoes non-radiative recombination with 100% probability if it reaches the effective radius, R . The appearance of the 2.1 eV band at 100 K and higher temperatures clearly indicates that there is a non-zero probability that a STE can still undergo intrinsic recombination in the highly defective core region. Indeed, the SiO_4 tetrahedron is a highly stable and indestructible element of the glass network and it is quite reasonable to assume that, even in highly damaged silica, there will always be possibility of STE recombination.

4. Conclusions

A model was developed to explain observed ion and temperature dependences of the 2.1 eV luminescence emission of silica under high electronic excitation ion irradiation at temperatures between 30 and 100 K. The model is found to quantitatively account for the main features observed in the experimental data. It also provides deep insight into the complex and rapid process of STE formation, migration, and recombination in silica exposed to swift ions. At the lowest temperatures measured, STEs are immobile, and their yield is governed primarily by the competition between Auger recombination and STE formation. For heavy ions, the inelastic thermal spike also appears to suppress STE formation at the center of the ion track. One of the remarkable predictions of the model is the formation of a STE halo around the track core. At elevated temperatures, the luminescence yield is largely controlled by STE hopping. A surviving STE can diffuse either to the center of the defective track core where it is likely to be quenched through non-radiative recombination process or outwards towards other defects in the glass network. The results are consistent with an activation energy for migration of around 0.12 eV. A key assumption of this work is that the Auger recombination coefficient of insulators correlates strongly with relative permittivity. It will be interesting to see what this model, or models similar to it, predict for insulators with large and small dielectric constants.

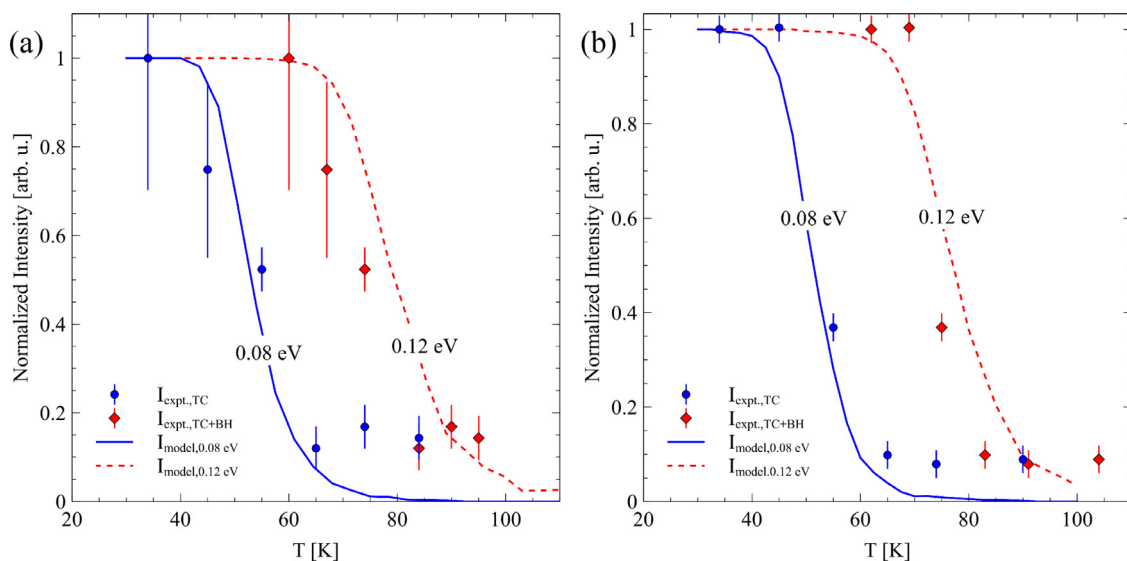


Fig. 8. The temperature dependence of the luminescence yield from the 2.1 eV emission band for 19 MeV Si ions (a) and 19 MeV Cl ions (b). The blue markers show the data plotted vs. the measured temperature on the cryostat (TC). The red markers include the beam heating correction (TC+BH). The lines indicate model predictions assuming STE migration energies of 0.08 eV (solid blue) and 0.12 eV (dashed red). Error bars represent the standard error.

Funding

This work has been supported by the [University of Tennessee Governor's Chair](#) program. M.L.C. also acknowledges financial support from the research project "Captacion de Talento UAM" Ref: #541D300 supervised by the Vice-Chancellor of Research of Universidad Autonoma de Madrid (UAM).

Data availability statement

The data that support the findings of this study are available from the corresponding author upon reasonable request.

Declaration of Competing Interest

The authors declare that they have no known competing financial interests or personal relationships that could have appeared to influence the work reported in this paper.

Appendices

A. beam heating temperature correction

As shown in [47], the beam heating effect can be significant for thermal insulators. As the present work is concerned with properties of fused silica, a thermal insulator, neglecting a temperature shift of even a few degrees at cryogenic temperature can lead to a misinterpretation of the results. The thermal conductivity of fused silica exhibits a strong temperature dependence at cryogenic temperatures [96,97]. Calculation of the beam heating effect through direct application of the simple analytical formula in ref. [47] is not possible as the temperature-dependent thermal conductivity makes the steady state heat equation non-linear, i.e.

$$\nabla \cdot [k(T)\nabla T] = \dot{q} \quad (\text{A.1})$$

Such non-linearities generally require the use of numerical solutions. However, in the temperature range of 20–100 K, the thermal conductivity of amorphous silica is approximately linear in temperature,

$$k(T) = \alpha T \quad (\text{A.2})$$

allowing one to recast the non-linear problem as an effective linear problem using a transformation of variables. Substituting Eq. A.2 into Eq. A.1 gives

$$\nabla \cdot [\alpha T \nabla T] = \dot{q} \quad (\text{A.3})$$

$$\frac{\alpha}{2} \nabla^2 T^2 = \dot{q} \quad (\text{A.4})$$

By making the variable transformations

$$\frac{\alpha}{2} \rightarrow k' \quad (\text{A.5})$$

$$T^2 \rightarrow T' \quad (\text{A.6})$$

one arrives a linear heat equation.

$$k' \nabla^2 T' = \dot{q} \quad (\text{A.7})$$

Using the results from ref. [47], one finds that for a semi-infinite slab, with negligible losses due to radiative and convective heat transfer, the temperature distribution on the surface is given by

$$T^2(x, y, z) = \Delta T^2(x, y, z) + T_0^2 \quad (\text{A.8})$$

T_0 is the temperature far away from the irradiation spot. This corresponds to the temperature measured by the thermocouple on the cryostat. The maximum temperature produced by the beam

Table A.1

Measured and corrected irradiation temperatures in degrees Kelvin.

3 MeV H		3.5 MeV He		19 MeV Si		19 MeV Cl	
T_0	T_{max}	T_0	T_{max}	T_0	T_{max}	T_0	T_{max}
33	45	36	77	34	60	34	62
45	55	45	82	45	67	45	69
		55	87	55	74	55	75
		65	94	65	84	65	83
		75	101	75	90	74	91
		85	109	84	95	90	104
		95	117				
		106	126				

heating effect for a square beam centered at $(x, y) = (0, 0)$ is given by

$$T_{max}^2 = T^2(0, 0, 0) = \frac{2\phi E l}{\pi \alpha} \ln \left(\frac{\sqrt{2} + 1}{\sqrt{2} - 1} \right) + T_0^2 \quad (\text{A.9})$$

where ϕ is the ion flux, E is the ion energy, and l is the side length of the square irradiation spot. Using the experimental values of Smith et al. [97] gives a best fit coefficient of $\alpha = 4.11 \times 10^{-3} \text{ W m}^{-1} \text{ K}^{-2}$.

Table A.1 gives the measured thermocouple temperatures (T_0) and the corrected temperatures in the irradiated spot (T_{max}). Note that the maximum temperatures only represent an upper bound. Because the 3.5 MeV helium irradiations used a RF plasma source instead of a solid cathode ion source, the ion flux was significantly greater for the 3.5 MeV He beam than for the other ions, hence the larger heating effect.

B. derivation of the STE dissociation rate constant

The formation of STE's and their dissociation occurs through the following equation



which is at equilibrium with a heat bath of an electron-hole plasma. Following a similar approach used in the derivation of the Saha equation [98], one equates the most probable states of the left hand and right-hand sides.

$$\frac{W_{STE} Z_{STE}}{N_{STE}} = \frac{W_{STH} Z_{STH}}{N_{STH}} \frac{W_e Z_e}{N_e} \quad (\text{B.2})$$

Z_i are the one particle partition functions, W_i are the number of microstates per particle in a volume of material and N_i are the number of particles in the same volume. It is assumed that $Z_{STH} = Z_e = 1$. In other words, the free electron and self-trapped holes have no internal degrees of freedom and are in their ground states. This also establishes the zero of energy. The STE partition function is then

$$Z_{STE} = e^{E_b/kT} \quad (\text{B.3})$$

where E_b is the binding energy of the STE. The value of E_b is around 0.2 eV for quartz [95]. As the STE is mostly localized on an SiO_4 tetrahedron in both quartz and silica, one could expect a similar magnitude binding energy of silica. However, it should be mentioned that fused silica, with distributions of bond angles and bond lengths, has a distribution of binding energies rather than a single value [95]. It was observed that varying the binding energy from 0.1 to 0.3 eV in the simulations changed the final yields by less than 5%. Increasing the binding energy to 0.6 eV still only changed the yield by less than 22%. Thus, 0.2 eV was deemed to be a reasonable order-of-magnitude value, certainly for the purposes of this rudimentary model.

Unlike the STEs and STHs, which are frozen over the timescales of Auger recombination and STE formation, the free electrons can

move at considerable speeds. The microstates of the free electrons are given by the number of plane wave particle states in a box:

$$W_e = V(2\pi m_e^* kT/h^2)^{3/2} \quad (\text{B.4})$$

V is the volume of the box, m_e^* is the effective mass of the electron (about $0.4m_e$ [99]) and h is Planck's constant. In contrast to the electrons, the self-trapped holes and self-trapped electrons cannot be approximated as plane waves. The number of microstates is assumed to be the number of sites that the STEs can occupy.

$$W_{STE} = W_{STH} = \frac{V}{\Omega} = NV \quad (\text{B.5})$$

Ω is the volume per SiO_2 unit and N is the atomic number density. With some cancellations, one has

$$\frac{V e^{E_b/kT}}{N_{STE}} = \frac{V}{N_{STH}} \frac{V(2\pi m_e kT/h^2)^{3/2}}{N_e} \quad (\text{B.6})$$

One could consider vibrational degrees of freedom for the STE and STH, though there would also be a degree of cancellation between the left- and right-hand sides of in Eq. B.2, assuming that the vibrational degrees of freedom are similar for STEs and STHs. In terms of the number densities,

$$\frac{e^{E_b/kT}}{n_{STE}} = \frac{1}{n_{STH}} \frac{(2\pi m_e kT/h^2)^{3/2}}{n_e} \quad (\text{B.7})$$

giving the equilibrium constant

$$\Gamma = \frac{n_{STH} n_e}{n_{STE}} = (2\pi m_e kT/h^2)^{3/2} e^{-E_b/kT} \quad (\text{B.8})$$

Since the electrons and holes are produced in pairs, $n_{STH} = n_e = n_c$ and

$$\Gamma = \frac{n_c^2}{n_{STE}} = (2\pi m_e kT/h^2)^{3/2} e^{-E_b/kT} \quad (\text{B.9})$$

Resulting in the STE dissociation term appearing in Eq. (4).

$$\partial_t n_{STE}(r, t) = \frac{1}{\tau_{STE}} n_c - \frac{\Gamma}{\tau_{STE}} \frac{n_{STE}}{n_c} \quad (\text{B.10})$$

One can verify that Γ is indeed the equilibrium rate constant by setting $\partial_t n_{STE}(r, t) = 0$.

References

- [1] F. Agulló-López, C.R.A. Catlow, P.D. Townsend, Point Defects in Materials, Academic Press, London, 1988.
- [2] P.D. Townsend, M. Khanlary, D.E. Hole, Information obtainable from ion beam luminescence, Surf. Coat. Technol. 201 (2007) 8160.
- [3] P.D. Townsend, Variations on the use of ion beam luminescence, Nucl. Instrum. Methods Phys. Res. Sect. B Beam Interact. Mater. Atoms 286 (2012) 35.
- [4] K.J. McCarthy, J.G. López, D.J. Rey, B. Zurro, A. Ibarra, A. Bacio, M.A. Respalda, The response of several luminescent materials to KeV and MeV ions, J. Nucl. Mater. 340 (2005) 291.
- [5] S. Nagata, S. Yamamoto, A. Inouye, B. Tsuchiya, K. Toh, T. Shikama, Luminescence characteristics and defect formation in silica glasses under H and He ion irradiation, J. Nucl. Mater. 367-370 (2007) 1009.
- [6] S. Nagata, S. Yamamoto, K. Toh, B. Tsuchiya, N. Ohtsu, T. Shikama, H. Naramoto, Luminescence in SiO_2 induced by MeV energy proton irradiation, J. Nucl. Mater. 329-333 (2004) 1507.
- [7] S.I. Kononenko, O.V. Kalantaryan, V.I. Muratov, V.P. Zhurenko, Silica luminescence induced by fast light ions, Radiat. Meas. 42 (2007) 751.
- [8] D. Jimenez-Rey, O. Peña-Rodríguez, J. Manzano-Santamaría, J. Olivares, A. Muñoz-Martín, A. Rivera, F. Agulló-López, Ionoluminescence induced by swift heavy ions in silica and quartz: a comparative analysis, Nucl. Instrum. Methods Phys. Res. Sect. B Beam Interact. Mater. Atoms 286 (2012) 282.
- [9] O. Peña-Rodríguez, D. Jiménez-Rey, J. Manzano-Santamaría, J. Olivares, A.P. Muñoz, A. Rivera, F. Agulló-López, Ionoluminescence as sensor of structural disorder in crystalline SiO_2 : determination of amorphization threshold by swift heavy ions, Appl. Phys. Express 5 (2012) 11101.
- [10] M.L. Crespillo, J.T. Graham, Y. Zhang, W.J. Weber, In-Situ luminescence monitoring of ion-induced damage evolution in SiO_2 and Al_2O_3 , J. Lumin. 172 (2016) 208-218.
- [11] L. Tong, R.R. Gattass, J.B. Ashcom, S. He, J. Lou, M. Shen, I. Maxwell, E. Mazur, Subwavelength-diameter silica wires for low-loss optical wave guiding, Nature 426 (2003) 816.
- [12] M. Lancry, B. Pommellec, UV laser processing and multiphoton absorption processes in optical telecommunication fiber materials, Phys. Rep. 523 (2013) 207.
- [13] J. Manzano, J. Olivares, F. Agulló-López, M.L. Crespillo, A. Morono, E. Hodgson, Optical waveguides obtained by swift-ion irradiation on silica ($\alpha\text{-SiO}_2$), Nucl. Instrum. Methods Phys. Res. Sect. B Beam Interact. Mater. Atoms 268 (2010) 3147.
- [14] M.L. Green, E.P. Gusev, R. Degraeve, E.L. Garfunkel, Ultrathin (<4 Nm) SiO_2 and Si-O-N gate dielectric layers for silicon microelectronics: understanding the processing, structure, and physical and electrical limits, J. Appl. Phys. 90 (2001) 2057.
- [15] edited by M.L. Reed, G.K. Fedder, T. Fukuda, W. Menz, 2 - Photolithographic microfabrication, in: Handbook of Sensors and Actuators, 6, Elsevier Science, 1998, pp. 13-61. edited by B.V..
- [16] J. Bude, C.W. Carr, P.E. Miller, T. Parham, P. Whitman, M. Monticelli, R. Raman, D. Cross, B. Welay, F. Ravizza, T. Suratwala, J. Davis, M. Fischer, R. Hawley, H. Lee, M. Matthews, M. Norton, M. Nostrand, D. VanBlarcom, S. Sommer, Particle damage sources for fused silica optics and their mitigation on high energy laser systems, Opt. Express 25 (2017) 11414.
- [17] W.J. Weber, R.C. Ewing, C.A. Angell, G.W. Arnold, A.N. Cormack, J.M. Delaye, D.L. Griscom, L.W. Hobbs, A. Navrotsky, D.L. Price, A.M. Stoneham, M.C. Weinberg, Radiation effects in glasses used for immobilization of high-level waste and plutonium disposition, J. Mater. Res. 12 (1997) 1948.
- [18] W.J. Weber, R.C. Ewing, C.R.A. Catlow, T.D. de la Rubia, L.W. Hobbs, C. Kinoshita, H. Matzke, A.T. Motta, M. Nastasi, E.K.H. Salje, E.R. Vance, S.J. Zinkle, Radiation effects in crystalline ceramics for the immobilization of high-level nuclear waste and plutonium, J. Mater. Res. 13 (1998) 1434.
- [19] J.F. Latkowski, A. Kubota, M.J. Caturla, S.N. Dixit, J.A. Speth, S.A. Payne, Fused silica final optics for inertial fusion energy: radiation studies and system-level analysis, Fusion Sci. Technol. 43 (2003) 540.
- [20] A. Morono, E.R. Hodgson, Radiation induced optical absorption and radioluminescence in electron irradiated SiO_2 , J. Nucl. Mater. 258-263 (1998) 1889.
- [21] A. Ibarra, E.R. Hodgson, The ITER project: the role of insulators, Nucl. Instrum. Methods Phys. Res. Sect. B Beam Interact. Mater. Atoms 218 (2004) 29.
- [22] M. Decretton, T. Shikama, E. Hodgson, Performance of functional materials and components in a fusion reactor: the issue of radiation effects in ceramics and glass materials for diagnostics, J. Nucl. Mater. 329-333 (2004) 125.
- [23] K. Tanimura, T. Tanaka, N. Itoh, Creation of quasistable lattice defects by electronic excitation in SiO_2 , Phys. Rev. Lett. 51 (1983) 423.
- [24] C. Itoh, K. Tanimura, N. Itoh, Optical studies of self-trapped excitons in SiO_2 , J. Phys. C Solid State Phys. 21 (1988) 4693.
- [25] D.L. Griscom, γ and fission-reactor radiation effects on the visible-range transparency of aluminum-jacketed, all-silica optical fibers, J. Appl. Phys. 80 (1996) 2142.
- [26] C.D. Marshall, J.A. Speth, S.A. Payne, Induced Optical absorption in gamma, neutron and ultraviolet irradiated fused quartz and silica, J Non Cryst. Solids 212 (1997) 59.
- [27] L. Skuja, M. Hirano, H. Hosono, K. Kajihara, Defects in oxide glasses, Phys. Status Solidi (c) 2 (2005) 15.
- [28] J.M. Costantini, F. Brisard, G. Biotteau, E. Balanzat, B. Gervais, Self-trapped exciton luminescence induced in alpha quartz by swift heavy ion irradiations, J. Appl. Phys. 88 (2000) 1339.
- [29] M. Ma, X. Chen, K. Yang, X. Yang, Y. Sun, Y. Jin, Z. Zhu, Color center formation in silica glass induced by high energy Fe and Xe ions, Nucl. Instrum. Methods Phys. Res. Sect. B Beam Interact. Mater. Atoms 268 (2010) 67.
- [30] J. Manzano-Santamaría, J. Olivares, A. Rivera, O. Peña-Rodríguez, F. Agulló-López, Kinetics of color center formation in silica irradiated with swift heavy ions: thresholding and formation efficiency, Appl. Phys. Lett. 101 (2012) 154103.
- [31] D. Bachiller-Perea, D. Jiménez-Rey, A. Muñoz-Martín, F. Agulló-López, Exciton mechanisms and modeling of the ionoluminescence in silica, J. Phys. D Appl. Phys. 49 (2016) 085501.
- [32] P. Martin, D. Jimenez-Rey, R. Vila, F. Sánchez, R. Saavedra, Optical absorption defects created in SiO_2 by Si, O and He ion irradiation, Fusion Eng. Des. 89 (2014) 1679.
- [33] L. Skuja, K. Kajihara, M. Hirano, H. Hosono, Oxygen-excess-related point defects in glassy/amorphous SiO_2 and related materials, Nucl. Instrum. Methods Phys. Res. Sect. B Beam Interact. Mater. Atoms 286 (2012) 159.
- [34] M. Fujiwara, T. Tanabe, H. Miyamaru, K. Miyazaki, Ion-induced luminescence of silica glasses, Nucl. Instrum. Methods Phys. Res. Sect. B Beam Interact. Mater. Atoms 116 (1996) 536.
- [35] K. Moritani, I. Takagi, H. Moriyama, Production behavior of irradiation defects in vitreous silica under ion beam irradiation, J. Nucl. Mater. 312 (2003) 97.
- [36] T. Yoshida, T. Ii, T. Tanabe, H. Yoshida, K. Yamaguchi, In Situ luminescence and optical absorption measurements of silica in reactor core, J. Nucl. Mater. 307-311 (2002) 1268.
- [37] K. Okamoto, K. Toh, S. Nagata, B. Tsuchiya, T. Suzuki, N. Shamoto, T. Shikama, Temperature dependence of radiation induced optical transmission loss in fused silica core optical fibers, J. Nucl. Mater. 329-333 (2004) 1503.
- [38] S. Nagata, S. Yamamoto, K. Toh, B. Tsuchiya, N. Ohtsu, T. Shikama, H. Naramoto, Luminescence in SiO_2 induced by MeV energy proton irradiation, J. Nucl. Mater. 329-333 (2004) 1507.
- [39] P.J. Chandler, F. Jaque, P.D. Townsend, Ion beam induced luminescence in fused silica, Radiat. Eff. 42 (1979) 45.
- [40] A. Rivera, J. Olivares, A. Prada, M.L. Crespillo, M.J. Caturla, E.M. Bringa, J.M. Perlado, O. Peña-Rodríguez, Permanent modifications in silica produced by ion-in-

- duced high electronic excitation: experiments and atomistic simulations, *Sci. Rep.* 7 (2017) 10641.
- [41] N. Itoh, D.M. Duffy, S. Khakshouri, A.M. Stoneham, Making tracks: electronic excitation roles in forming swift heavy ion tracks, *J. Phys. Condens. Matter* 21 (2009) 474205.
- [42] F. Agulló-López, A. Climent-Font, Á. Muñoz-Martín, J. Olivares, A. Zucchiatti, Ion beam modification of dielectric materials in the electronic excitation regime: cumulative and exciton models, *Prog. Mater. Sci.* 76 (2016) 1.
- [43] A. Trukhin, *Silicon Dioxide and the Luminescence of Related Materials: Crystal Polymorphism and the Glass State*, Cambridge Scholars Publishing, Newcastle upon Tyne, 2021.
- [44] N. Itoh, Self-trapped exciton model of heavy-ion track registration, *Nucl. Instrum. Methods Phys. Res. Sect. B Beam Interact. Mater. Atoms* 116 (1996) 33.
- [45] Y. Zhang, M.L. Crespillo, H. Xue, K. Jin, C.H. Chen, C.L. Fontana, J.T. Graham, W.J. Weber, New ion beam materials laboratory for materials modification and irradiation effects research, *Nucl. Instrum. Methods Phys. Res. Sect. B Beam Interact. Mater. Atoms* 338 (2014) 19–30.
- [46] M.L. Crespillo, J.T. Graham, F. Agulló-López, Y. Zhang, W.J. Weber, Role of oxygen vacancies on light emission mechanisms in SrTiO₃ induced by high-energy particles, *J. Phys D Appl Phys* 50 (2017) 155303.
- [47] M.L. Crespillo, J.T. Graham, Y. Zhang, W.J. Weber, Temperature measurements during high flux ion beam irradiations, *Rev. Sci. Instrum.* 87 (2016) 024902.
- [48] M. Wojdyr, Fityk: a general-purpose peak fitting program, *J. Appl. Crystallogr.* 43 (2010) 1126.
- [49] J. Wolberg, *Data Analysis Using the Method of Least Squares: Extracting the Most Information from Experiments*, Springer, 2006.
- [50] J. Jagielski, L. Thomé, Multi-step damage accumulation in irradiated crystals, *Appl. Phys. A* 97 (2009) 147.
- [51] F.S. Ham, Stress-assisted precipitation on dislocations, *J. Appl. Phys.* 30 (1959) 915.
- [52] B.J. Luff, P.D. Townsend, Cathodoluminescence of synthetic quartz, *J. Phys. Condens. Matter* 2 (1990) 8089.
- [53] X. Zhang, C.K. Ong, Hole trapping properties of germanium in alpha -quartz, *J. Phys. Condens. Matter* 7 (1995) 1603.
- [54] R.M. van Ginhoven, H. Jónsson, L.R. Corrales, Characterization of exciton self-trapping in amorphous silica, *J. Non Cryst. Solids* 352 (2006) 2589.
- [55] J.M. Costantini, F. Brisard, G. Biotteau, L. Protin, Luminescence of SiO₂ quartz induced by swift heavy ion irradiations, *J. Non Cryst. Solids* 216 (1997) 36.
- [56] C.T. Kirk, Quantitative analysis of the effect of disorder-induced mode coupling on infrared absorption in silica, *Phys. Rev. B* 38 (1988) 1255.
- [57] S.N. Taraskin, S.R. Elliott, Nature of vibrational excitations in vitreous silica, *Phys. Rev. B* 56 (1997) 8605.
- [58] B. Hehlen, G. Simon, The vibrations of vitreous silica observed in hyper-raman scattering, *J. Raman Spectrosc.* 43 (2012) 1941.
- [59] E.L. Galeener, A.J. Leadbetter, M.W. Stringfellow, Comparison of the Neutron, Raman, and Infrared Vibrational Spectra of Vitreous SiO₂, GeO₂, and BeF₂, *Phys. Rev. B* 27 (1983) 1052.
- [60] R. Sahl, Defect Related Luminescence in Silicon Dioxide Network: a Review, in: S. Basu (Ed.), *Crystalline Silicon - Properties and Uses*, IntechOpen, IntechOpen, Rijeka, 2011.
- [61] L. Muga, G. Griffith, Specific luminescence studies in plastic scintillators, *Phys. Rev. B* 9 (1974) 3639.
- [62] K. Michaelian, A. Menchaca-Rocha, Model of ion-induced luminescence based on energy deposition by secondary electrons, *Phys. Rev. B* 49 (1994) 15550.
- [63] E.S. Goulding, Y. Stone, Semiconductor radiation detectors, *Science* 170 (1970) 280.
- [64] R. Katz, D.E. Dunn, G.L. Sinclair, Thindown in radiobiology, *Radiat Prot Dosim.* 13 (1985) 281.
- [65] M.P.R. Waligórski, R.N. Hamm, R. Katz, The radial distribution of dose around the path of a heavy ion in liquid water, *Int. J. Radiat. Appl. Instrum. Part D* 11 (1986) 309.
- [66] O. Fageeha, J. Howard, R.C. Block, Distribution of radial energy deposition around the track of energetic charged particles in silicon, *J. Appl. Phys.* 75 (1994) 2317.
- [67] A.M. Goodman, Electron hall effect in silicon dioxide, *Phys. Rev.* 164 (1967) 1145.
- [68] R.C. Hughes, Charge-carrier transport phenomena in amorphous SiO₂: direct measurement of the drift mobility and lifetime, *Phys. Rev. Lett.* 30 (1973) 1333.
- [69] Z.A. Weinberg, W.C. Johnson, M.A. Lampert, Determination of the sign of carrier transported across SiO₂ Films on Si, *Appl. Phys. Lett.* 25 (1974) 42.
- [70] T.H. DiStefano, D.E. Eastman, Photoemission Measurements of the valence levels of amorphous SiO₂, *Phys. Rev. Lett.* 27 (1971) 1560.
- [71] R.C. Hughes, Hole mobility and transport in thin SiO₂ films, *Appl. Phys. Lett.* 26 (1975) 436.
- [72] P. Jürgens, M.J.J. Vrakking, A. Husakou, R. Stoian, A. Mermillod-Blondin, Plasma Formation and relaxation dynamics in fused silica driven by femtosecond short-wavelength infrared laser pulses, *Appl. Phys. Lett.* 115 (2019) 191903.
- [73] P. Audebert, Ph. Daguzan, A. dos Santos, J.C. Gauthier, J.P. Geindre, S. Guizard, G. Hamoniaux, K. Krastev, P. Martin, G. Petite, A. Antonetti, Space-time observation of an electron gas in SiO₂, *Phys. Rev. Lett.* 73 (1994) 1990.
- [74] P. Martin, S. Guizard, Ph. Daguzan, G. Petite, P. D'Oliveira, P. Meynadier, M. Perdrix, Subpicosecond study of carrier trapping dynamics in wide-band-gap crystals, *Phys. Rev. B* 55 (1997) 5799.
- [75] M. Li, S. Menon, J.P. Nibarger, G.N. Gibson, Ultrafast electron dynamics in femtosecond optical breakdown of dielectrics, *Phys. Rev. Lett.* 82 (1999) 2394.
- [76] M. Mero, J. Liu, A. Sabbah, J. C. Jasapara, K. Starke, D. Ristau, J. K. McIver, W. G. Rudolph, Femtosecond pulse damage and predamage behavior of dielectric thin films, *SPIE Proceedings vol. 4932, Laser-Induced Damage in Optical Materials: 2002 and 7th International Workshop on Laser Beam and Optics Characterization* (2003) 202–216.
- [77] Q. Sun, H. Jiang, Y. Liu, Z. Wu, H. Yang, Q. Gong, Measurement of the collision time of dense electronic plasma induced by a femtosecond laser in fused silica, *Opt. Lett.* 30 (2005) 320.
- [78] C. Pan, L. Jiang, Q. Wang, J. Sun, G. Wang, Y. Lu, Temporal-spatial measurement of electron relaxation time in femtosecond laser induced plasma using two-color pump-probe imaging technique, *Appl. Phys. Lett.* 112 (2018) 191101.
- [79] D. Grojo, M. Gertsvolf, S. Lei, T. Barillot, D.M. Rayner, P.B. Corkum, Exciton-seeded multiphoton ionization in bulk SiO₂, *Phys. Rev. B* 81 (2010) 212301.
- [80] K.A. Bulashevich, S. Yu. Karpov, Is Auger recombination responsible for the efficiency rollover in III-nitride light-emitting diodes? *Phys. Status Solidi C* 5 (2008) 2066.
- [81] K.G. Svantesson, N.G. Nilsson, The temperature dependence of the Auger recombination coefficient of undoped silicon, *J. Phys. C Solid State Phys.* 12 (1979) 5111.
- [82] Y. Yamada, H. Yasuda, T. Tayagaki, Y. Kanemitsu, Temperature dependence of photoluminescence spectra of nondoped and electron-doped SrTiO₃: crossover from Auger recombination to single-carrier trapping, *Phys. Rev. Lett.* 102 (2009) 247401.
- [83] Y. Yamada, K. Suzuki, Y. Kanemitsu, Blue photoluminescence and auger recombination of carriers in SrTiO₃ nanoparticles, *Appl. Phys. Lett.* 99 (2011) 093101.
- [84] F. de Rougemont, R. Frey, P. Roussignol, D. Ricard, C. Flytzanis, Evidence of strong auger recombination in semiconductor-doped glasses, *Appl. Phys. Lett.* 50 (1987) 1619.
- [85] C. Wehrenfennig, G.E. Eperon, M.B. Johnston, H.J. Snaith, L.M. Herz, High charge carrier mobilities and lifetimes in organolead trihalide perovskites, *Adv. Mater.* 26 (2014) 1584.
- [86] J.M. Richter, M. Abdi-Jalebi, A. Sadhanala, M. Tabachnyk, J.P.H. Rivett, L.M. Pazos-Outón, K.C. Gödel, M. Price, F. Deschler, R.H. Friend, Enhancing photoluminescence yields in lead halide perovskites by photon recycling and light out-coupling, *Nat. Commun.* 7 (2016) 13941.
- [87] J. Fu, Q. Xu, G. Han, B. Wu, C.H.A. Huan, M.L. Leek, T.C. Sum, Hot carrier cooling mechanisms in halide perovskites, *Nat. Commun.* 8 (2017) 1300.
- [88] Y. Yang, M. Yang, Z. Li, R. Crisp, K. Zhu, M.C. Beard, Comparison of recombination dynamics in CH₃NH₃PbBr₃ and CH₃NH₃PbI₃ perovskite films: influence of exciton binding energy, *J. Phys. Chem. Lett.* 6 (2015) 4688.
- [89] A.A. Sirenko, C. Bernhard, A. Golnik, A.M. Clark, J. Hao, W. Si, X.X. Xi, Soft-mode hardening in SrTiO₃ thin films, *Nature* 404 (2000) 373.
- [90] M. Stengel, N.A. Spaldin, Origin of the dielectric dead layer in nanoscale capacitors, *Nature* 443 (2006) 679.
- [91] C. Dufour, B. Lesellier de Chezelles, V. Delignon, M. Toulemonde, E. Paumier, P. Mazzoldi, A transient thermodynamic model for track formation in amorphous semi-conductor: a possible mechanism? in: *On Chemical and Physical Modifications Induced by Irradiation in Glasses*, 126, E-MRS, Strasbourg, 1992, p. 61.
- [92] A. Benyagoub, M. Toulemonde, Ion tracks in amorphous silica, *J. Mater. Res.* 30 (2015) 1529.
- [93] S. al Smairat, J. Graham, Vacancy-induced enhancement of electron-phonon coupling in cubic silicon carbide and its relationship to the two-temperature model, *J. Appl. Phys.* 130 (2021) 125902.
- [94] J.F. Ziegler, M.D. Ziegler, J.P. Biersack, SRIM – The stopping and range of ions in matter (2010), *Nucl. Instrum. Methods Phys. Res. Sect. B Beam Interact. Mater. Atoms* 268 (2010) 1818.
- [95] edited by A.N. Trukhin, G. Pacchioni, L. Skuja, D.L. Griscom, Excitons, localized states in silicon dioxide and related crystals and glasses, in: *Defects in SiO₂ and Related Dielectrics: Science and Technology*, Springer, Dordrecht, Netherlands, 2000, pp. 235–283, edited by.
- [96] R. Berman, F.E. Simon, The thermal conductivities of some dielectric solids at low temperatures (experimental), *Proc. R. Soc. Lond. Ser A Math. Phys. Sci.* 208 (1951) 90.
- [97] T.L. Smith, P.J. Anthony, A.C. Anderson, Effect of neutron irradiation on the density of low-energy excitations in vitreous silica, *Phys. Rev. B* 17 (1978) 4997.
- [98] M.N. SAHA, Ionisation in the solar chromosphere, *Nature* 105 (1920) 232.
- [99] M. Lenzlinger, E.H. Snow, Fowler-nordheim tunneling into thermally grown SiO₂, *J. Appl. Phys.* 40 (1969) 278.